SUPPORTING INFORMATION

Fluorescent conjugated mesoporous polymers with *N*, *N*-diethylpropylamine for efficient capture and real-time detection of volatile iodine

Meiyun Xu [a], Tao Wang [a], Lei Zhou [a], Daoben Hua [a,b,*]

[a] State Key Laboratory of Radiation Medicine and Protection, School of Radiological and Interdisciplinary Sciences (RAD-X), Soochow University, Suzhou 215123, China; correspondence to: dbhua_lab@suda.edu.cn;

[b] Collaborative Innovation Center of Radiological Medicine of Jiangsu Higher Education Institutions, Suzhou 215123, China.

Table of contents

1. Materials and characterization

1,3-dibromopropane (Shanghai Macklin Biochemical Co., Ltd, CP), ethylenediamine, diethylamine, trifluoromethanesulfonic acid, CuI, Trimethylsilylacetylene 2,7-dibromo-9H-fluorene (BePharm Ltd), tetrakis(triphenylphosphine)-palladium (0) [$Pd(PPh_3)_4$] (Energy Chemical Reagent Co., Ltd, CP), sodium carbonate anhydrous and N,N-dimethylformamide (DMF) (Sinopharm Chemical Reagent Co., Ltd, CP), were used as received. Ultrapure water used in the all experiments was obtained from Milli-Q water purification system (Milli-pore Corporation, USA).

X-ray photoelectron spectroscopy (XPS) was carried out by an ESCALAB 250Xi spectrometer. Fourier transform infrared (FTIR) spectra were recorded on a Varian-1000 spectrometer. Solid-state ^{13}C CP/MAS NMR and ^{1}H NMR measurements were carried out on a Bruker Avance III model 400 MHz NMR spectrometer at a MAS rate of 5 kHz. Surface areas and pore size distributions were measured by N_2 and CO_2 sorption and desorption at 77.3 K and 273 K, respectively, using the ASAP 2020 volumetric sorption analyzer. BET surface areas were calculated over the relative pressure range 0.05-0.15 P/P_0. Samples were degassed at 100 °C for 10 h under high vacuum before analysis. Thermogravimetric analysis (TGA) was performed on TG/DTA 6300 in air or N_2 flow. Powder X-ray diffraction (XRD) patterns were obtained on a Bruker D8 Advance diffractometer (40 kV, 30 Ma) using Cu Kα radiation ($2\theta = 3°\sim90°$). Electron spin resonance (ESR) measurements were conducted at room temperature on a JES-X320 ESR spectrometer using a thin-walled capillary tube (3 mm o.d.) loading with 5 cm length of sample powders (scan mode: microwave power of 3.0 mW, 3000−4000 G, one scan). Transmission electron microscopy (TEM) was performed on a Tecnai G2 spirit BioTwin field emission scanning electron microscope. ^{60}Co gamma-ray irradiation was carried out at ^{60}Co radiation laboratory of

Soochow University. The dose rate was 2.6 kGy/h. β ray irradiation was conducted on a RHODOTRONTT 200 type electron accelerator made by IBA company, Belgium.

2. Synthesis of monomer F2

2, 7-dibromo-9, 9'-bis(3-bromopropyl)-fluorene (F1) were prepared according to reported literatures (Figure S1) (Elemental Analysis: Calcd for C, 40.32%; H, 3.21%; Br, 56.47%; Found C, 40.57%; H, 3.60%; MS (TOF) m/z: [F1] Calcd for C19H18Br4 561.81; Found 561.73).[1, 2] F1 (1.2 g, 2.12 mmol) was dissolved in 15 mL acetone, and then ethylenediamine (20 eq, 84.8 mmol), K_2CO_3 (2.00 g, 14.47 mmol) and KI (0.20 g, 1.20 mmol) were added. The mixture was stirred at 60 ^oC under N_2 overnight. After cooling down to room temperature, the precipitate was filtered, and the filtrate was concentrated under vacuum. The residue was dissolved with 3 mL ethanol, and precipitated with water. The white precipitate was collected through filter, and dried in vacuum. The white precipitate was collected through filter, and dried in vacuum to give a white solid (0.91g, 82%). 1H NMR ($CDCl_3$, 400 MHz), δ 7.52-7.45 (6H, m), 2.70 (4H, t, J = 5.6 Hz), 2.48 (4H, t, J = 5.6 Hz), 2.37 (4H, t, J = 7.0 Hz), 1.99 (4H, t, J = 7.8 Hz), 0.80-0.77 (4H, m). Elemental Analysis: Calcd for C, 52.69%; H, 6.15%; Br, 30.48%; N, 10.69%; Found C, 50.32%; H, 6.61%; N, 9.80; MS (TOF) m/z: [F2+H]+ Calcd for C23H33Br2N4 523.11; Found 523.29.

3. Synthesis of monomer F3

F1 (1.20 g, 2.12 mmol) was dissolved in 12 mL acetone, and then diethylamine (9 eq, 19.08 mmol), K_2CO_3 (2.00 g, 14.47 mmol) and KI (0.20 g, 1.20 mmol) were added. The mixture was stirred at 60 ^oC under N_2 overnight. After cooling down to room temperature, the precipitate was filtered, and the filtrate was concentrated under vacuum. The residue was dissolved in CH_2Cl_2, and then washed with water three times. The combined organic layer was dried over anhydrous Na_2SO_4. CH_2Cl_2 was removed in vacuo, and the desired product F2 was obtained as a white solid (1.08 g, 99%). 1H NMR ($CDCl_3$, 400 MHz), δ 7.52-7.43 (6H, m), 2.28 (8H, q, *J* = 7.2 Hz), 2.14 (4H, t, *J* = 7.6 Hz), 1.95 (4H, t, *J* = 8.0 Hz), 0.86 (12H, t, *J* = 7.2 Hz), 0.78-0.71 (4H, m). Elemental Analysis: Calcd for C, C, 58.92%; H, 6.96%; Br, 29.03%; N, 5.09%; Found C, 58.99%; H, 7.12%; N, 5.02; MS (TOF) m/z: [F3+H]+ Calcd for C27H39Br2N2 549.15; Found 549.06.

4. Sorption kinetics

Pseudo-first-order equation is described as followed (S1):

$$\log(q_\mathrm{e} - q_\mathrm{t}) = \log q_\mathrm{e} - (\frac{k_1}{2.303}) \times t \qquad \text{(S1)}$$

where q_e and q_t (mg/g) are the sorption capacity of U(VI) at equilibrium time and contact time t [min], respectively, and k_1 [min^{-1}] represents the pseudo first order kinetic constant. q_e and k_1 can be calculated from the slope and intercept of the plot of log (q_e-q_t) versus t, respectively (Figure S10A).

Pseudo-second-order model is expressed as the following Equation (S2):

$$\frac{t}{q_\mathrm{t}} = \frac{1}{k_2 \times q_\mathrm{e}^2} + \frac{t}{q_\mathrm{e}} \qquad \text{(S2)}$$

where k_2 [g/mg/min] represents the rate constant of the pseudo-second order model, and can be determined from the plot of t/q_t against t (Figure S10B).

5. Iodine vapor pressure

The iodine vapor pressure at different temperature was calculated according to the Antoine formula (S3) as follow:

$$lgP = A - B/(T + C) \qquad \text{(S3)}$$

where A, B, C are the constants of different substances (for iodine, A=7.26304, B=1697.87, C=204.000), T ($^\mathrm{o}$C) is the corresponding temperature, P (mm mercury column) is the vapor pressure of substance.

Table S1. XPS Binding Energies, Fitting Parameters FWHM for CMPs.

Element	Material	Assignment	Binding energy (eV)	FWHM*	Area
C 1s	CMPH	C≡C	286.9	2.2	7616
		triazine	285.5	0.9	9245
		π-π	284.7	1.1	41511
		C-C	284.0	1.1	5077
	$CMPNH_2$	C≡C	286.9	2.0	4555
		triazine	285.7	1.1	6056
		π-π	284.9	1.0	14076
		C-N	284.6	0.8	4766
		C-C	284.1	1.0	8825
	CMPN	C≡C	286.9	1.6	4184
		triazine	285.6	1.3	8255
		π-π	284.9	1.0	27337
		C-N	284.6	0.5	4801
		C-C	284.1	0.8	12760
N 1s	CMPH	triazine	398.9	1.2	4607
	$CMPNH_2$	Hydrogen bonded NH/NH_2	400.5	1.0	1319
		NH, NH_2	399.9	1.26	3002
		triazine	398.9	1.4	3112
	CMPN	C-N	400.2	3.1	4160
		triazine	398.9	1.2	3770

*: full width at half maximum.

Table S2. Kinetic parameters for iodine vapor sorption on CMPs at 75°C.

Sorbent	$q_{e,exp}$ (g/g)	Pseudo-first-order			Pseudo-second-order		
		k_1 (h^{-1})	$q_{e,cal}$ (mg/g)	R^2	k_2 (g/h/mg)	$q_{e,cal}$ (mg/g)	R^2
CMPH	1.95	0.162	1.07	0.875	0.253	1.99	0.998
CMPNH$_2$	2.83	0.237	1.03	0.776	0.121	2.87	1.000
CMPN	5.02	0.255	2.53	0.906	0.313	5.14	1.000

Table S3. Summary of surface area, heteroatom content and iodine sorption properties of CMPs.

Sorbent (heteroatom)	BET (m^2 g^{-1})	T (°C)	Heteroatom content (%)	Iodine uptake (g g^{-1})	Reference
TTPPA (N)	512	77	14.86	4.90	J. Mater. Chem. A, 2018, 6, 2808
TTPA (N)	308	77	15.81	4.92	Micropor. Mesopor. Mat., 2019, 273,163
Azo-Trip (N)	510.4	77	12.96	2.38	Polym. Chem., 2016, 7, 643
CMPNs	1368	70	-	2.08	J. Mater. Chem. A, 2015,3, 87-91
SCMP-2 (S)	855	80	-	2.22	ACS Appl. Mater. Interfaces, 2016, 8, 21063
FCMP-600@4 (F)	636	77	-	1.41	Sci. Rep., 2017, 7, 13972
SCMP-II (S)	119.76	80	-	3.45	Chem. Commun., 2016, 52, 9797
TTPB (N)	222	77	13.38	4.43	J. Mater. Chem. A, 2017, 5, 7612
AzoPPN (N)	400	77	-	2.90	Chem. Eur. J. 2016, 22, 11863
BDP-CPP-1	635	75	-	2.83	J. Mater. Chem. A, 2017, 5, 6622
CMP-LS5 (N)	1185	80	-	4.40	Polym. Chem., 2019, 10, 2608
HCMP-3 (N)	50/82	85	-	3.36	Macromolecules 2016, 49, 6322
POP-2 (N)	41	80	-	3.82	J Hazard. Mater. 2017, 338, 224
CMOP-1(N)	431	80	18.17	1.60	Molecules 2018, 23, 1732
CMPN	86.2	85	8.096	5.03	This work

Table S4. Kinetic parameters for iodine molecule sorption on CMPH, $CMPNH_2$ and CMPN in hexane at room temperature.

Sorbent	$q_{e,exp}$ (g/g)	Pseudo-first-order			Pseudo-second-order		
		k_1 (min^{-1})	$q_{e,cal}$ (mg/g)	R^2	k_2 (g/min/mg)	$q_{e,cal}$ (mg/g)	R^2
CMPH	0.028	0.0271	0.018	0.927	3.965	0.034	0.997
$CMPNH_2$	0.295	0.0125	0.227	0.977	0.112	0.318	1.000
CMPN	0.299	0.0412	0.092	0.902	2.039	0.302	1.000

Table S5. Kinetic parameters for iodine vapor sorption on CMPN at different temperature.

Sorbent	$q_{e,exp}$ (g/g)	Pseudo-first-order			Pseudo-second-order		
		k_1 (h^{-1})	$q_{e,cal}$ (mg/g)	R^2	k_2 (g/h/mg)	$q_{e,cal}$ (mg/g)	R^2
298 K	3.89	0.013	1.40	0.703	0.048	3.93	1.000
318 K	3.99	0.056	1.22	0.808	0.191	4.03	1.000
333 K	5.09	0.133	2.90	0.898	0.186	5.16	0.997
358 K	5.03	0.330	1.05	0.717	1.332	5.07	1.000

Table S6. The peak shifts of FT-IR spectra of parents and iodine-loaded CMPN.

Assignment	CMPN	CMPN-I_2	shift
Benzene stretch	1603 cm^{-1}	1568 cm^{-1}	35 cm^{-1}
	1504 cm^{-1}	1496 cm^{-1}	8 cm^{-1}
Triazine stretch	1566 cm^{-1}	1537 cm^{-1}	29 cm^{-1}
	1359 cm^{-1}	1350 cm^{-1}	9 cm^{-1}
C–N stretch	1296 cm^{-1}	1270 cm^{-1}	26 cm^{-1}
C-H bending	815 cm^{-1}	796 cm^{-1}	19 cm^{-1}

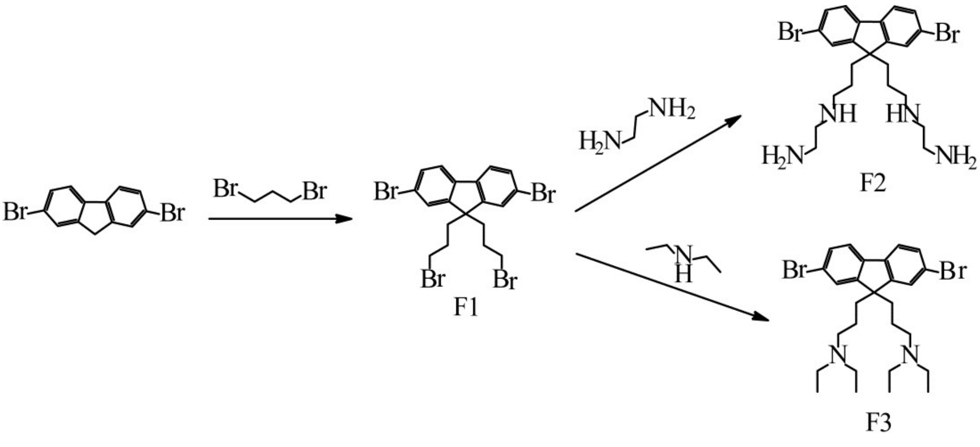

Figure S1. The synthetic route of monomers.

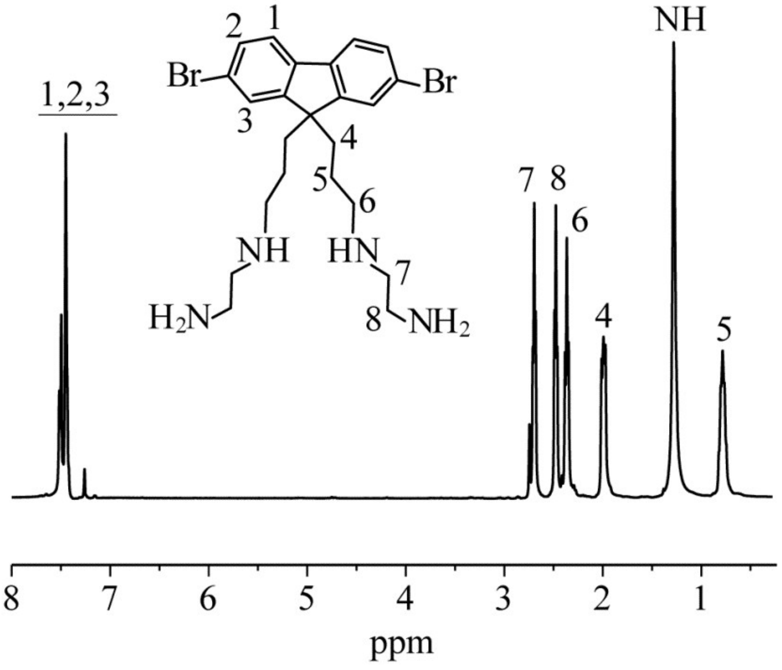

Figure S2. ^{1}H NMR spectrum of F2 in CDCl$_3$.

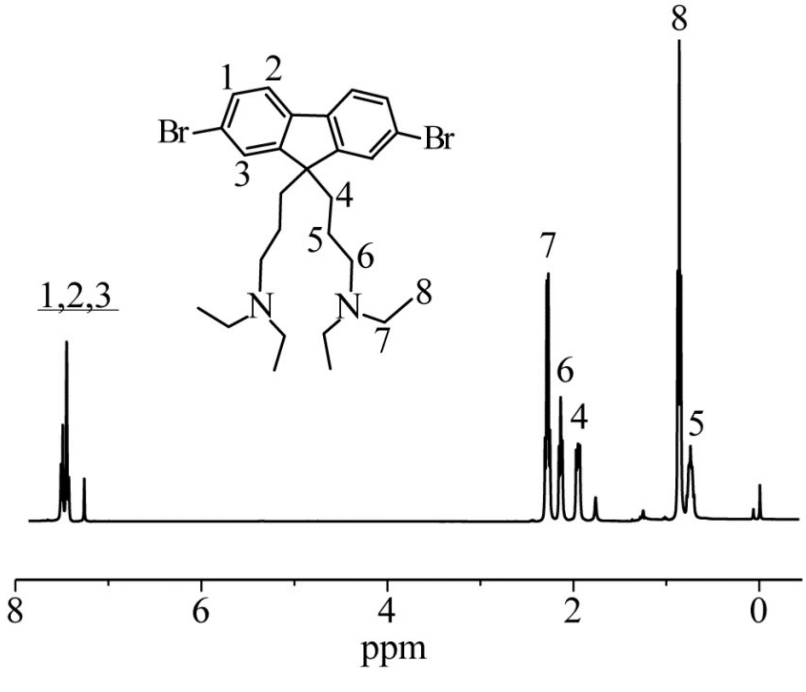

Figure S3. ^{1}H NMR spectrum of F3 in CDCl$_3$.

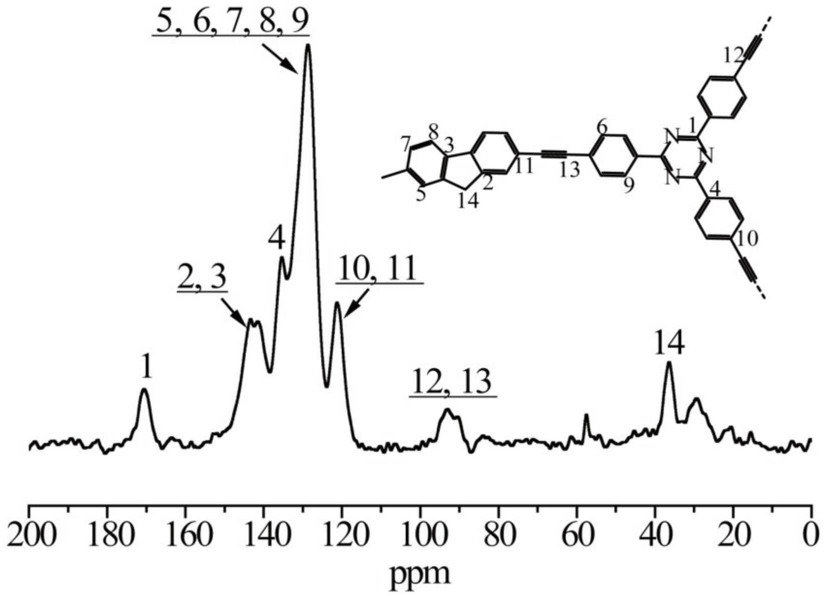

Figure S4. Solid-state ^{13}C NMR spectrum of CMPH.

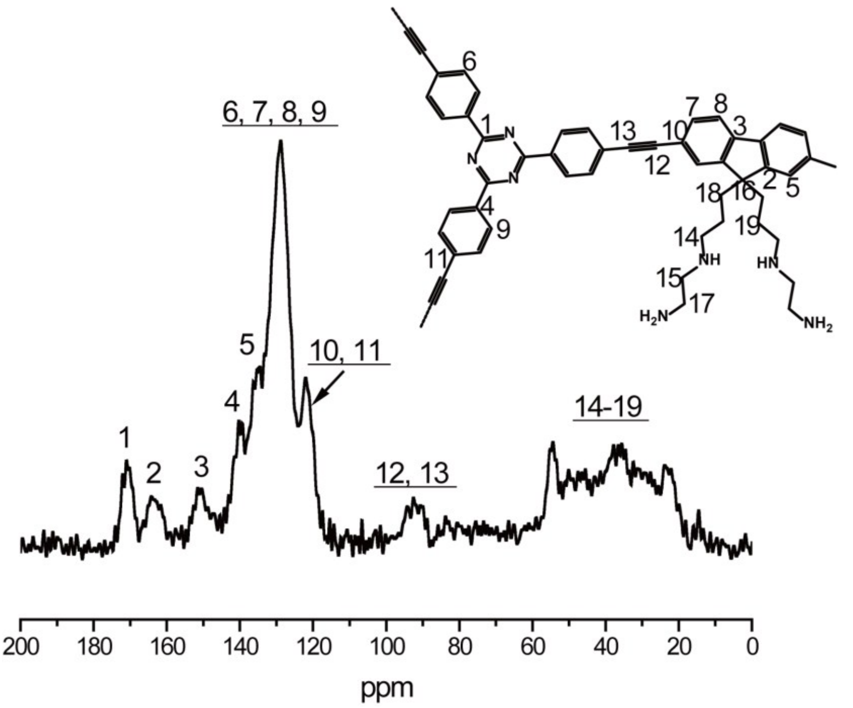

Figure S5. Solid-state ^{13}C NMR spectrum of CMPNH$_2$.

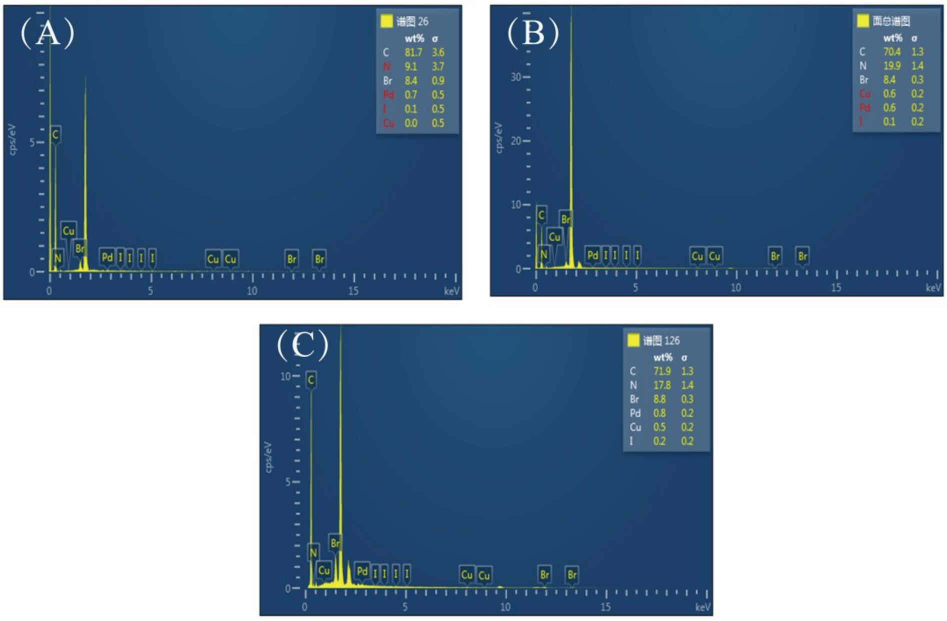

Figure S6. EDS spectra of (A) CMPH, (B) $CMPNH_2$ and (C) CMPN.

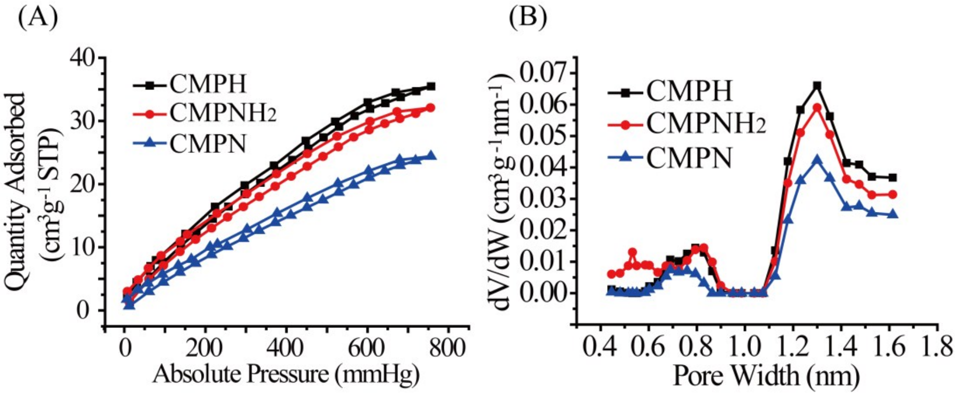

Figure S7. (A) CO_2 sorption/desorption isotherms and (B) pore size distribution of CMPs.

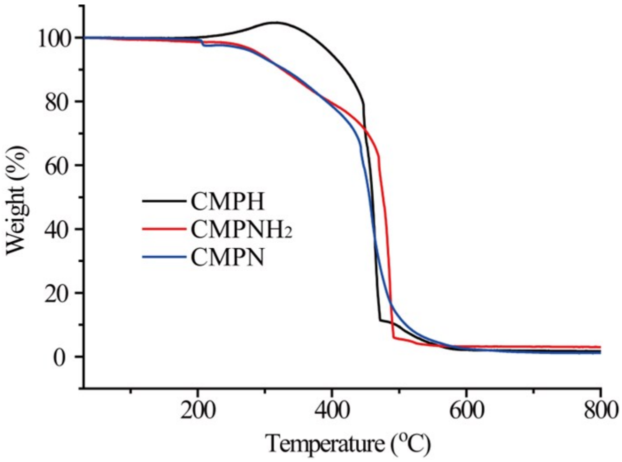

Figure S8. TGA analysis of materials under atmosphere.

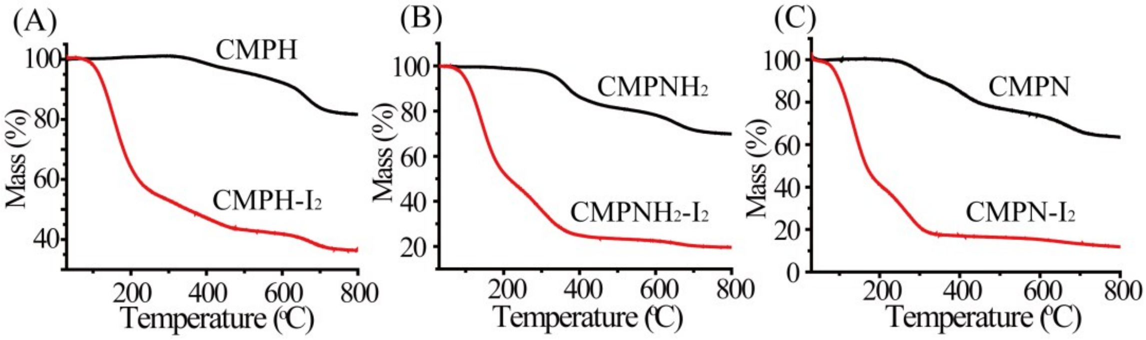

Figure S9. TGA analysis of CMPs and iodine loaded CMPs under N_2.

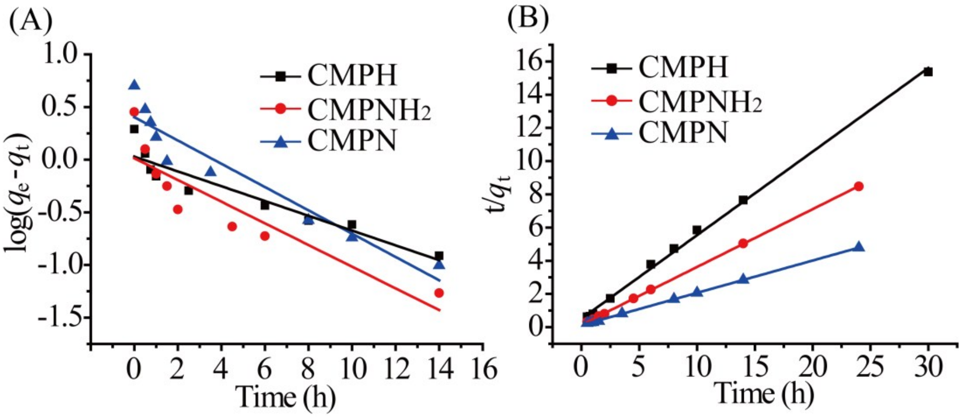

Figure S10. (A) Pseudo-first order kinetics and (B) Pseudo-second order kinetics of iodine vapor sorption at 75 ^{o}C.

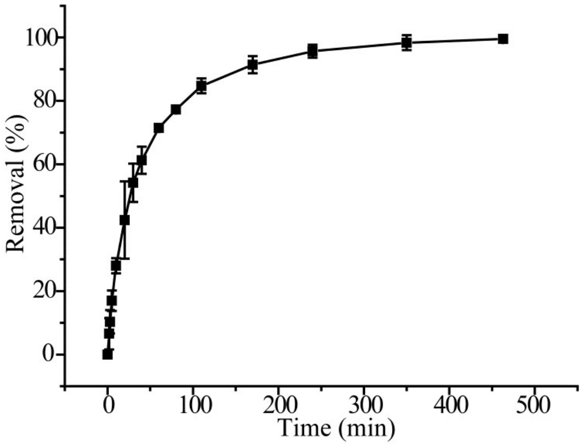

Figure S11. Removal for dissolved iodine of $CMPNH_2$ as a function of time in hexane solutions (Experiment conditions: $C_{sorbent}$ = 1.0 mg/mL, C_{iodine} = 0.3 mg/mL, T=25^{o}C).

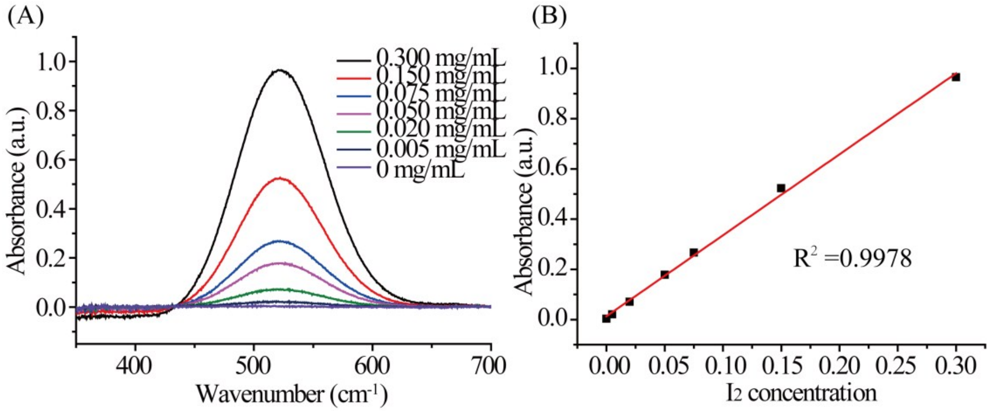

Figure S12. (a) Calibration plot of standard iodine by UV-Vis spectra in hexane solution. (b) The fitting of Abs value *vs* concentration of I_2 with the relatively good linearity satisfies Lambert-Beer Law.

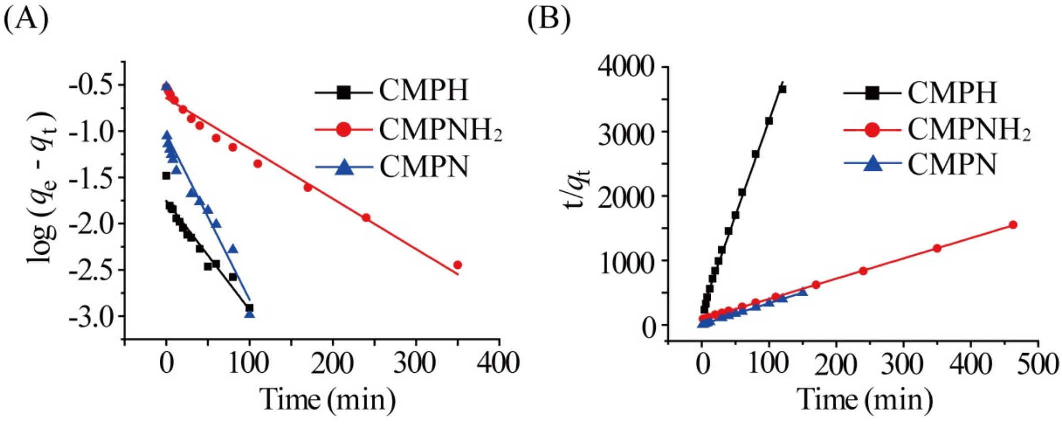

Figure 13. (A) Pseudo-first order kinetics and (B) Pseudo-second order kinetics of iodine vapor sorption in hexane at 25°C.

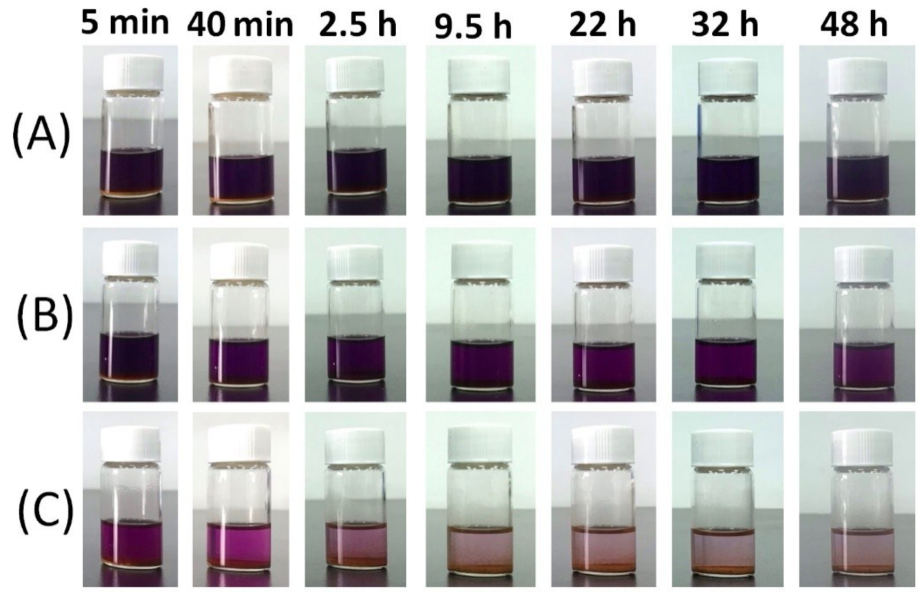

Figure S14. Images of iodine adsorption by (A) CMPH, (B) CMPNH$_2$, and (C) CMPN as a function of time in hexane solutions (Experiment conditions: C_{sorbent} = 1.0 mg/mL, C_{iodine} = 2.0 mg/mL, T=25$^{\mathrm{o}}$C).

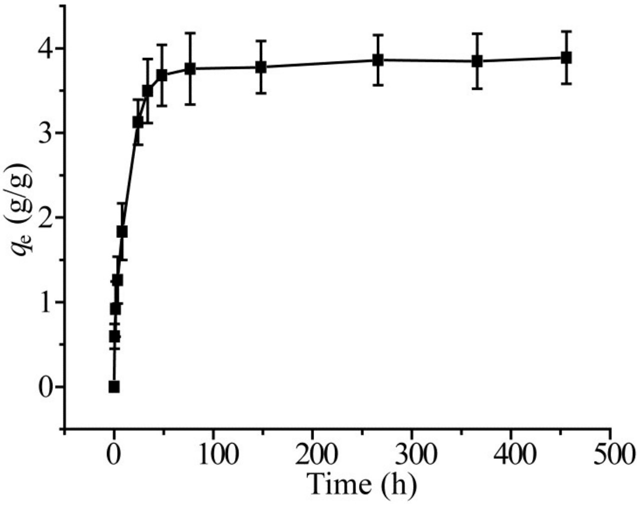

Figure S15. Gravimetric iodine uptake of CMPN as a function of time at 25 $^{\mathrm{o}}$C.

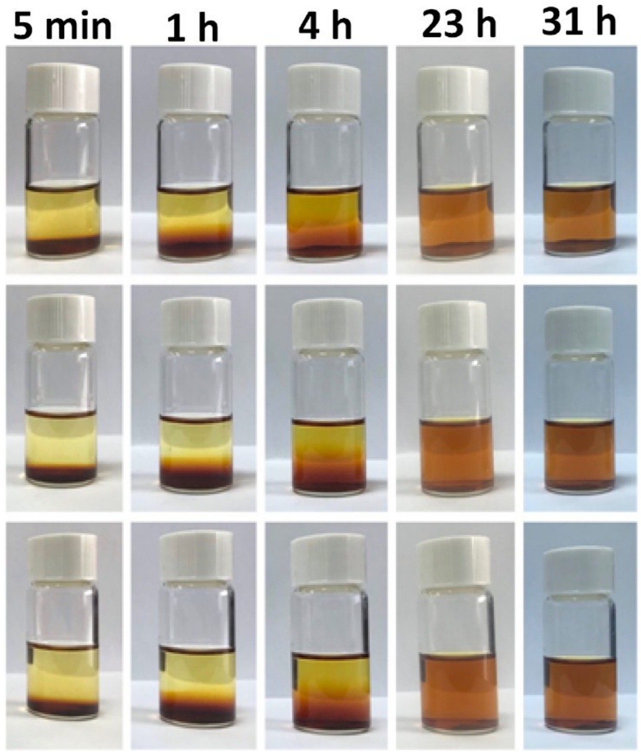

Figure S16. Release of iodine from the CMPN@I_2 in EtOH.

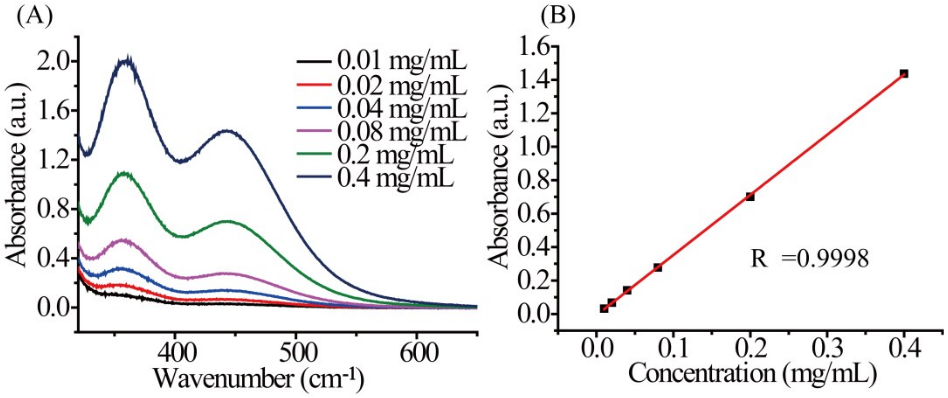

Figure S17. (a) Calibration plot of standard iodine by UV-Vis spectra in ethanol solution. (b) The fitting of Abs value *vs* concentration of I_2 with the relatively good linearity satisfies Lambert-Beer Law.

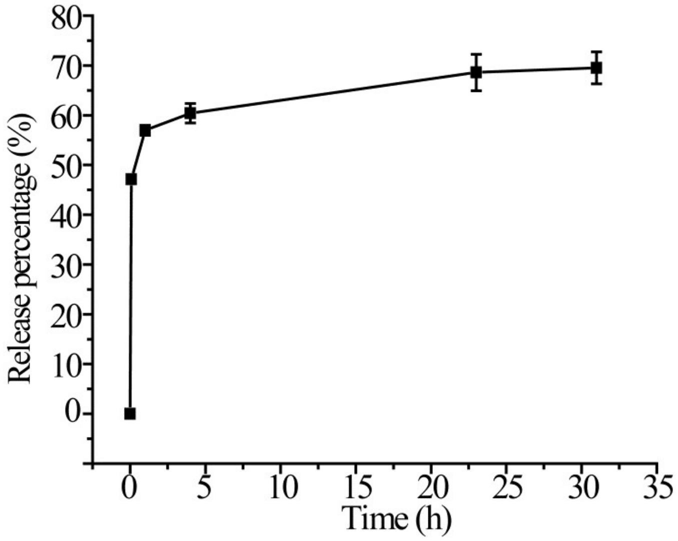

Figure S18. The release curves of the loaded I_2 from CMPN in EtOH.

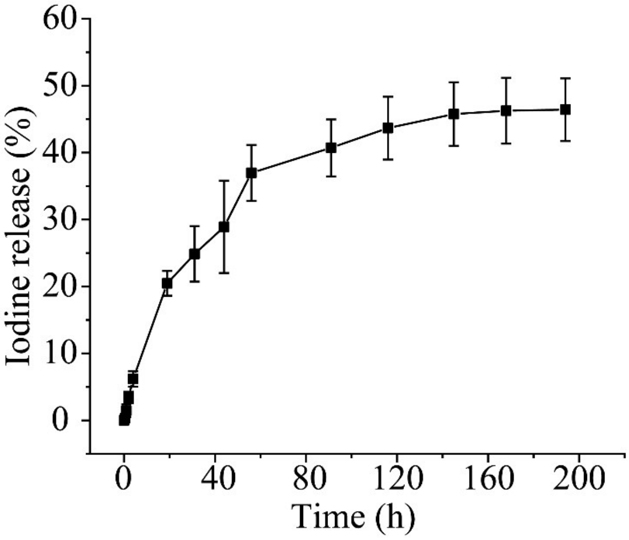

Figure S19. The release curves of the loaded I_2 from CMPN at 25°C.

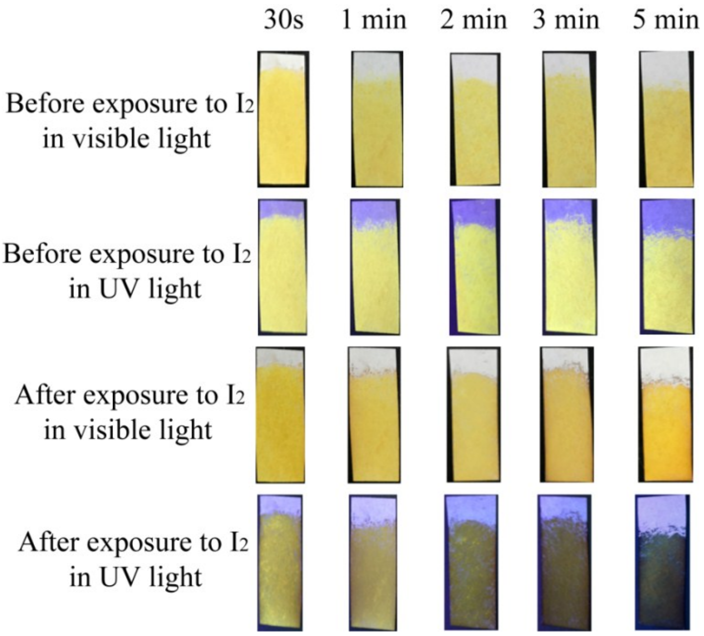

Figure S20. The images of testing paper before and after exposure to iodine vapor.

References

1. B. Liu, B. S. Gaylord, S. Wang and G. C. Bazan, *Journal of the American Chemical Society*, 2003, **125**, 6705.
2. C. Chi, A. Mikhailovsky and G. C. Bazan, *Journal of the American Chemical Society*, 2007, **129**, 11134.